

Energy extraction of a chaotic system in a cyclic process: a Szilárd Engine perspective

Artur Soriani¹ and Marcus V. S. Bonança²

Instituto de Física ‘Gleb Wataghin’, Universidade Estadual de Campinas, 13083-859, Campinas, São Paulo, Brazil

E-mail: ¹ a164189@dac.unicamp.br
² mbonanca@ifi.unicamp.br

Abstract. Inspired by the available examples of Microcanonical Szilárd Engines and by the original Szilárd Engine, we devise a system with two degrees of freedom whose ensemble average energy, starting with a microcanonical ensemble, decreases after a cyclic variation of its external parameters. We use the Ergodic Adiabatic Theorem to motivate our cycle and numerical simulations to check the decrement in the average energy. We then compare our system to the aforementioned Szilárd Engines, Microcanonical or not, and speculate about symmetry breaking being the cause of energy extraction in cyclic processes, even when non-integrability and chaos are present.

Keywords: Ergodicity breaking, Numerical simulations, Nonlinear dynamics.

1. Introduction

In 1871, James Clerk Maxwell described a simple thermodynamic system that, by the action of an intelligent being with access to the microscopic state of the system, would violate the Second Law of Thermodynamics, as it was understood [1]. This intelligent being, later named Maxwell's Demon, seemed like an odd supposition, as microscopic information is never available to us. Later, in 1929, Leo Szilárd proposed a cleaner version of Maxwell's Demon, one where the demon is simplified to an external agent that, based on a measurement made on a system in contact with a single thermal reservoir, exerts a cyclic thermodynamic process on this system and extracts energy from it, going against the Kelvin-Planck statement of the second law. Szilárd's engine [2], as Szilárd's thought experiment became known, gives us a more quantifiable version of Maxwell's Demon and one where the importance of information is fully flashed out.

Szilárd's original engine is simple, but ingenious. Consider a one particle gas inside a box connected to a heat reservoir, ensuring that processes the gas goes through are isothermal. At some point, a barrier is inserted in the middle of the box so as to divide it in two parts and the particle gets trapped in one of the sides. The insertion of the barrier, in principle, has no energy cost attached to it, or at least the energy cost can be made arbitrarily small. A measure is then made to determine which side of the box the particle got trapped in. Knowing which side the particle is, we now let the barrier act as a piston and, by moving the barrier, the one particle gas expands or compresses, meanwhile the particle collides with the barrier and exerts pressure. More specifically, we let the gas expand quasi-statically to its full original volume and, while colliding with the barrier, the particle exerts work and loses energy. When the barrier reaches the end of the box, it is removed (also with no energy cost, like the barrier insertion) and the cycle is finished. Kelvin-Planck's statement of the second law says that *"it is impossible to devise a cyclically operating device, the sole effect of which is to absorb energy in the form of heat from a single thermal reservoir and to deliver an equivalent amount of work"*. But that is exactly what Szilárd's engine does: the whole cycle operates at constant temperature and the energy the particle loses can be extracted and stored (as potential energy of a weight, for example).

Later contributions by Landauer [3] and Bennett [4] led to the conclusion that the Second Law of Thermodynamics is still valid once the energetics of information storage and information erasure are considered. Finally, Sagawa and Ueda generalized these ideas [5, 6, 7, 8, 9]. They formulated the *Second Law of Information Thermodynamics*, where thermodynamic quantities and information quantities are treated on equal footing. In turn, the work by Sagawa and Ueda unfolded a myriad of other works [10, 11, 12, 13, 14, 15, 16] about the Thermodynamics of feedback processes (processes dependent on a previous measurement, like the original Szilárd Engine), and, in particular, we now have autonomous Maxwell demons [17, 18, 19, 20, 21], examples where the demon is itself a physical sub-system, part of a bigger system.

In recent years, there has been a resurgence of interest in the implementation of

different versions of Maxwell Demons, i.e. systems that, through use of measurement and information, defy certain statements of the Second Law of Thermodynamics. A quantum formulation of Szilárd's Engine [22] has only recently been developed. Experimental verifications of the relation between information and energy have also been made recently [23, 24, 25, 26]. It has even been shown, based on fluctuation theorems, that feedback processes constitute a kind of symmetry breaking on the system's phase-space and that this symmetry breaking is ultimately the mechanism that allows energy extraction from a single heat reservoir to happen [23, 27, 28], at least for processes carried out at constant temperature.

More important to the scope of this work are Maxwell Demons that start with microcanonically sampled initial conditions, instead of the isothermal condition always present in the original Szilárd Engine. For instance, Sato [29] provided an example of a one-dimensional system whose ensemble average energy, starting with a microcanonical ensemble, decreases after an operation. Later, Microcanonical Szilárd Engines were proposed [30, 31, 32], versions of the Szilárd Engine where it is possible to extract energy from a single heat reservoir in a cycle by using the information acquired from a measurement of the energy of the system (not position, like in the original Szilárd's Engine) in every realization of the cycle (not simply on average, like in Sato's example). It has yet to be proven whether or not symmetry breaking is responsible for energy extractions in Microcanonical Szilárd Engines. If it is, we expect more complex examples of this kind of engine to exist. For a quantum example of work extraction from a microcanonical bath in the thermodynamic limit, see reference [33].

This work is laid out as follows: in section 2, we describe the general thermodynamic cycle we use; in section 3, we present the specific Hamiltonian we work with; in section 4, we present the mechanical cycle described by the cyclic variation of the external parameters of said Hamiltonian; in section 5, we apply the Ergodic Adiabatic Theorem and numerical simulations to check the energy variations within the mechanical cycle; in section 6, we compare our model with other models and discuss its achievements; in section 7, we give our concluding remarks.

2. The thermodynamic cycle

In this work, we aim to provide a system with two degrees of freedom whose ensemble average energy, starting with a microcanonical ensemble, decreases after cyclic variation of its external parameters. Two degrees of freedom may not seem as much of an improvement from one, but it already introduces more complex dynamic concepts like non-integrability and chaos, which are present in most thermodynamic systems. Consider the following thermodynamic cycle:

1. We start with an equilibrium ensemble of our system with Hamiltonian H in contact with a heat reservoir at temperature T .
2. We disconnect each element of the ensemble from the reservoir. At this point, the ensemble in question is a canonical ensemble at temperature T .

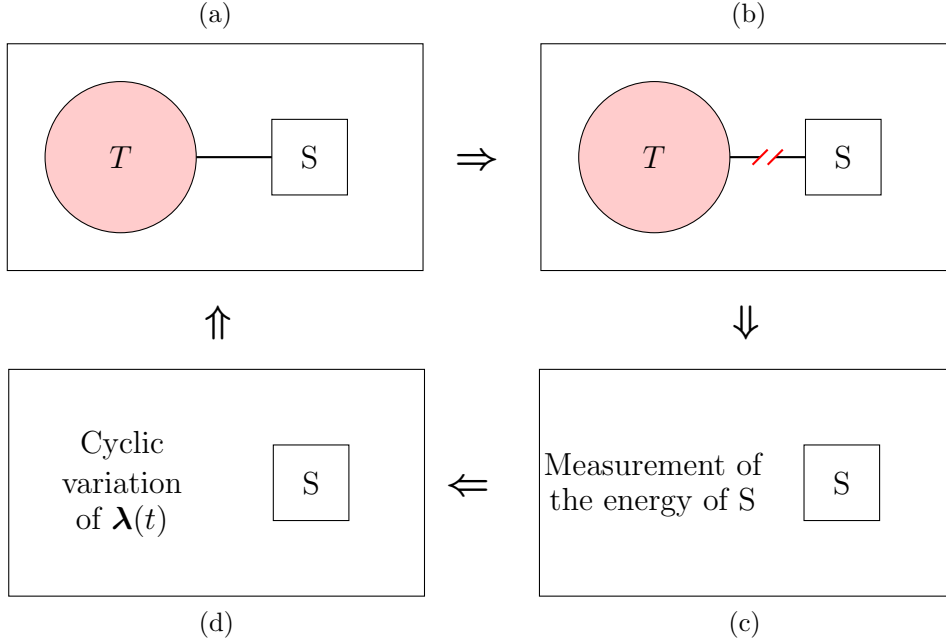


Figure 1. (Color online) Schematic representation of the thermodynamic cycle proposed. We start in the top left, panel (a), with each copy S of the system of our ensemble connected to heat reservoir at temperature T . We then disconnect S from the reservoir, on panel (b). Each element of our ensemble now occurs with probability given by the Boltzmann weight. Moving on to panel (c), we measure the energy of each element in the ensemble and organize them in microcanonical sub-ensembles of well defined energy. Given our mechanical cycle described by $\lambda(t)$, on panel (d) we submit it only on elements of sub-ensembles that have their average energy decreased after the mechanical cycle. Finally, we reconnect the whole initial ensemble with the heat reservoir, returning it to canonical equilibrium. This brings us back to panel (a) of the figure and finishes the thermodynamic cycle.

3. We measure the energy of each element in our ensemble and sort them according to the value E of energy measured. The result is then a set of sub-ensembles of well-defined energy, i.e., microcanonical sub-ensembles.
4. We implement a mechanical cycle in a given sub-ensemble *only if* its average energy *decreases* after it. By mechanical cycle, we mean a cyclic variation of external parameters λ in the system's Hamiltonian. The final result is a decrease of the average energy of the total ensemble since we have either decreased or left constant the average energies of the sub-ensembles.
5. We reconnect the ensemble with the heat reservoir and let it return to equilibrium.

This thermodynamic cycle is schematized in figure 1. It is obviously a cycle and the energy that the sub-ensemble loses during the cycle is extracted as work. We are transforming the energy absorbed of a single heat reservoir into work in a cycle, in clear contradiction to the Kelvin-Planck statement of the second law.

3. Working substance with two degrees of freedom

Our working substance will be given by the following QS Hamiltonian [34]

$$H^{\text{QS}}(\mathbf{z}, a) = \frac{p_x^2}{2} + \frac{p_y^2}{2} + \frac{a}{4} (x^4 + y^4) + \frac{x^2 y^2}{2}, \quad (1)$$

where QS stands for *quartic system*, $\mathbf{z} = (x, y, p_x, p_y)$ is a point in four-dimensional phase-space and a is an always positive external parameter responsible for determining the form of the potential well. When $a = 1$, the last two terms of equation (1) can be combined in a single term $\frac{(x^2 + y^2)^2}{4}$ and we have a central potential, which in turn means that angular momentum is conserved, serving as a second constant of motion (the first is the energy) and making the system integrable. On the other hand, when $0 < a < 1$, the system has only one constant of motion and is not integrable. In addition to that, for low values of a , like $a = 0.1$, the system can be considered ergodic for all practical purposes. Perhaps even more interestingly, a generic ensemble of this system with $a = 0.1$ has the property of auto-relaxation: when allowed to evolve by itself, it will relax to a microcanonical ensemble after time τ_R , called the relaxation time.

Poincaré sections of the system for different values of a are shown in figure 2. These are reduced two-dimensional phase spaces of the system that maintain all the characteristics that the original four-dimensional phase space has [35]. For $a = 1$ (figure 2a), all trajectories display complete regular behavior, as all of them are periodic and have constant angular momentum. There is a clear division between trajectories with positive angular momentum (in this case, with $x > 0$) and trajectories with negative angular momentum ($x < 0$). For $a = 0.5$ (figure 2b), we have a mixture of regular and irregular behavior: some trajectories are periodic, as can be seen in the four lobes with circular shapes, and some are not periodic, concentrated in the middle of the figure. For $a = 0.1$ (figure 2c), all the trajectories display approximately ergodic behavior, as all of the phase space points are well distributed over the entire surface.

To demonstrate the property of auto-relaxation, we sampled a microcanonical ensemble of the Hamiltonian of equation (1) with initial energy $E = 0.5$ for $a = 0.1$ and changed it abruptly to $a = 0.12$. The average kinetic and potential energies of this sampling are displayed in figure 3. In it, we can see that the ensemble relaxes to a microcanonical ensemble (with stationary averages in agreement with analytical calculations in the microcanonical ensemble, see Appendix A) again in less than 100 units of simulation time, so we can make $\tau_R = 100$. Since the dynamics of the Hamiltonian of equation (1) is scalable with energy (see equation (18) of reference [36]), so are its time scales and we can conclude that the relaxation time for other values of energy is $\tau_R(E') = \left(\frac{0.5}{E'}\right)^{1/4} 100$. This relaxation time serves as characteristic time scale of the Hamiltonian and any other time scale should be compared to it.

We want to make use of the separation between trajectories with positive and negative angular momentum, as shown in figure 2a, in order to extract energy from the system. However, cyclic variation of the parameter a in equation (1) is not enough, as Fermi acceleration phenomena with only one external parameter show [37]. To this end,

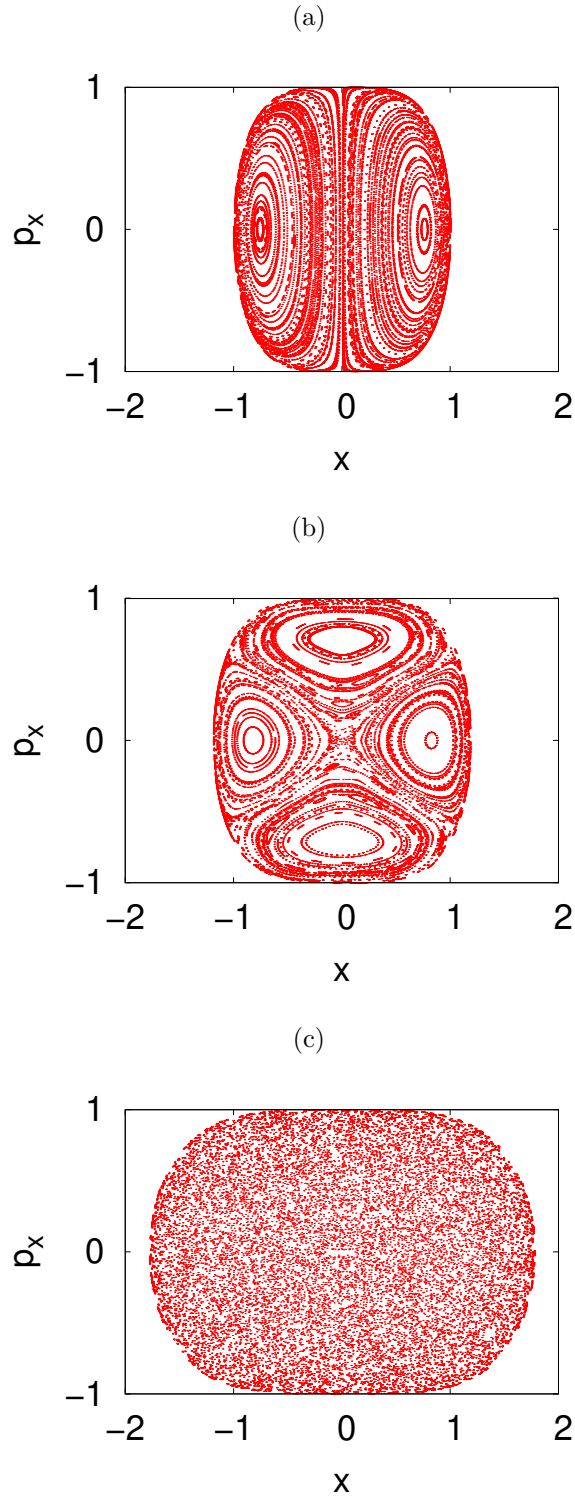


Figure 2. (Color online) Poincaré sections for the QS Hamiltonian of equation (1) in the plane $y = 0$ for $p_y > 0$ with $E = 0.5$ for (a) $a = 1$; (b) $a = 0.5$; (c) $a = 0.1$. These sections were obtained with the use of a symplectic numerical integrator [38], with 100 initial conditions and an elapsed time $\tau = 1000$. Figures 2a and 2b do not respect the reflection symmetry in the p_x axis, present in equation (1), because we did not use symmetrical initial conditions.

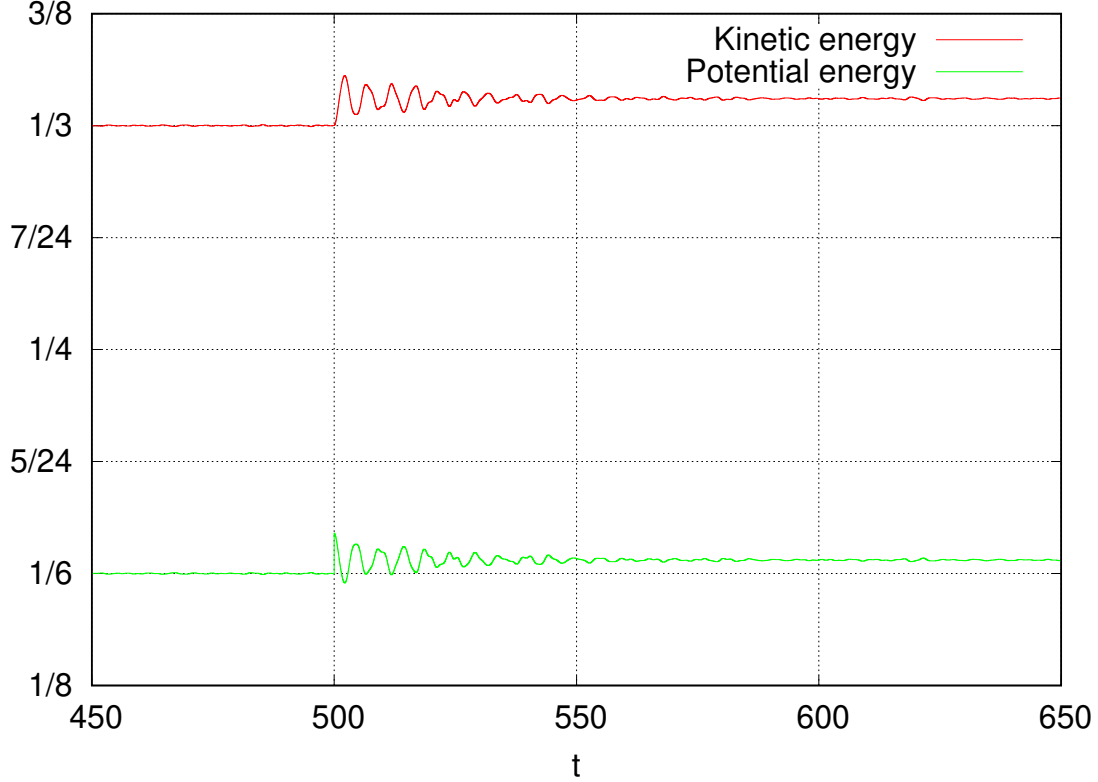


Figure 3. (Color online) Ensemble averages of kinetic and potential energies, the first two terms and the last two terms in equation (1), respectively. We sampled 10^6 initial conditions of the QS Hamiltonian with $E = 0.5$ and $a = 0.1$. We evolved this microcanonical ensemble with a symplectic numerical integrator [38] for 500 units of time, suddenly changed a from 0.1 to 0.12 and then let the system evolve for 500 more units of time. The system relaxes to a microcanonical state after less than 100 units of simulation time.

we add a term to equation (1) proportional to the angular momentum $L = xp_y - yp_x$,

$$H(\mathbf{z}, a, b) = \frac{p_x^2}{2} + \frac{p_y^2}{2} + \frac{a}{4} (x^4 + y^4) + \frac{x^2 y^2}{2} + b (xp_y - yp_x), \quad (2)$$

and manipulate a and b as we see fit. This newly added term $b(xp_y - yp_x)$, for any value of the external parameter b , does not interfere with the angular momentum conservation for $a = 1$.

4. The mechanical cycle

A mechanical cycle is implemented in this system by attributing temporal dependence to $a(t)$ and $b(t)$ during a time interval τ and making sure that $a(\tau) = a(0)$ and $b(\tau) = b(0)$. We have developed a feedback cycle that depends on a measurement of angular momentum of a given trajectory. The mechanical cycle we will use, divided in three steps, is as follows.

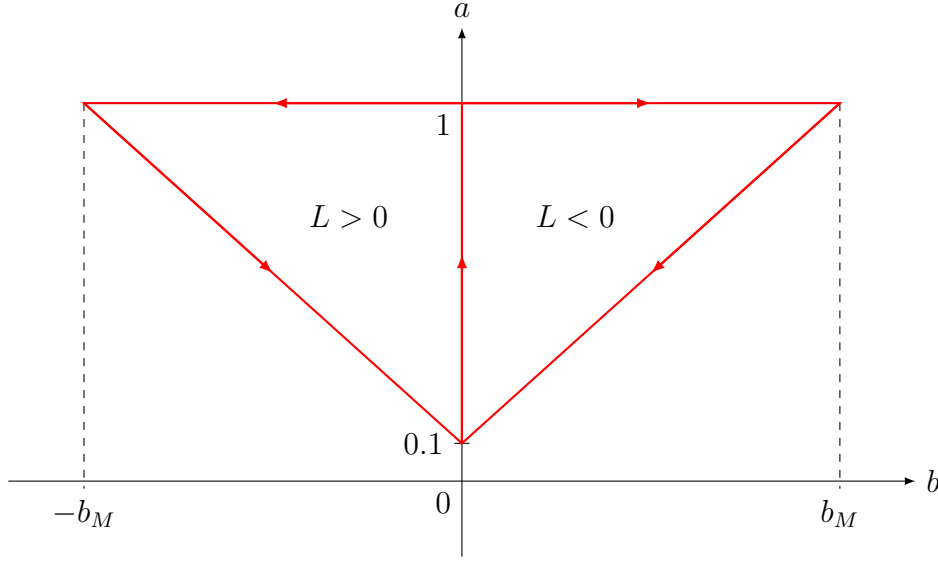


Figure 4. (Color online) Graphic representation of the protocols $a(t)$ and $b(t)$ to be implemented in the system of Hamiltonian given by equation (2). After a measurement of the angular momentum L of the trajectory when $a = 1$ and $b = 0$, we have two possible protocols: the one on the left for $L > 0$ and the one on the right for $L < 0$.

- (i) Starting with $a = 0.1$ and $b = 0$, in an ergodic regime, a increases linearly with time until it reaches $a = 1$ and b does not change, between times $t = 0$ and $t = \tau/4$;
- (ii) A measurement of the sign of the angular momentum L of the trajectory is made. Then, between times $t = \tau/4$ and $t = \tau/2$, a does not change and, if $L > 0$, b decreases linearly with time until it reaches $b = -b_M$, else if $L < 0$, b increases linearly with time until it reaches $b = b_M$, with $b_M > 0$;
- (iii) And finally, between $t = \tau/2$ and $t = \tau$, a decreases linearly with time from $a = 1$ to $a = 0.1$ and simultaneously b returns to its original value, 0, either from b_M or $-b_M$, finishing the mechanical cycle.

Or, more succinctly,

$$a(t) = \begin{cases} 0.1 + 0.9\frac{4t}{\tau}, & \text{if } 0 < t < \tau/4; \\ 1, & \text{if } \tau/4 < t < \tau/2; \\ 1.9 - 0.9\frac{2t}{\tau}, & \text{if } \tau/2 < t < \tau; \end{cases}$$

and

$$b(t) = \begin{cases} 0, & \text{if } 0 < t < \tau/4; \\ b_M \left(-1 + \frac{4t}{\tau}\right), & \text{if } \tau/4 < t < \tau/2; \\ b_M \left(2 - \frac{2t}{\tau}\right), & \text{if } \tau/2 < t < \tau. \end{cases}$$

A symmetry is clearly achieved and broken during this protocol: angular momentum conservation. This symmetry can be easily visualized in figure 2a, where trajectories of positive and negative angular momentum are well divided. Hence, the first step of this cycle, responsible for splitting the initial sub-ensemble in two regions of well defined

sign of angular momentum, is analogous to the barrier insertion in the Szilárd engine. The attainment and breaking of symmetry in our mechanical cycle is intentional and will be discussed in section 6. The most crucial step of our mechanical cycle is step 2, and it is the reason why we added the angular momentum term to equation (2). Step 2 is responsible for diminishing the ensemble's mean energy, and later in this section we will show exactly how.

We implement this mechanical cycle quasi-statically, which means $\tau \rightarrow \infty$ (or, realistically speaking, $\tau \gg \tau_R$), and make use of the Ergodic Adiabatic Theorem as an attempt to trace the energy variation of a trajectory in this mechanical cycle. The Ergodic Adiabatic Theorem states that the phase space volume $\Omega(E, \boldsymbol{\lambda})$ of a surface of constant energy $H(\mathbf{z}, \boldsymbol{\lambda}) = E$ ($\boldsymbol{\lambda}$ being a vector containing all the external parameters considered), given by

$$\Omega(E, \boldsymbol{\lambda}) = \int \Theta(E - H(\mathbf{z}, \boldsymbol{\lambda})) d\mathbf{z}, \quad (3)$$

where Θ is the Heaviside Theta function ($\theta(x) = 1$ if $x \geq 0$ and $\theta(x) = 0$ otherwise), is conserved during a process, as long as the process is quasi-static and the system remains ergodic throughout the entire process [39, 40]. However, our system does not meet the criteria for this theorem, as we know that our system is integrable for $a = 1$ and therefore not ergodic, but, as we will show, the theorem still gives us a decent prediction for the energy values, at least on average. In our case, $\boldsymbol{\lambda} = (a, b)$ and, even though equation (3) cannot be calculated explicitly for all values of a and b , it can be in a few specific cases. For example,

$$\Omega(E, a, 0) = \frac{16\pi}{3} \sqrt{\frac{2}{1-a}} E^{3/2} F \left(\sin^{-1} \sqrt{\frac{1-a}{1+a}} \middle| \frac{1+a}{1-a} \right), \quad (4)$$

where $F(\phi_0 | k^2) = \int_0^{\phi_0} \frac{d\phi}{(1-k^2 \sin^2 \phi)^{1/2}}$ is the incomplete elliptic integral of the first kind, and

$$\Omega(E, 1, b) = \frac{\pi^2}{3} \left((b^4 + 4E)^{3/2} + b^2 (b^4 + 6E) \right). \quad (5)$$

Both results agree when $a = 1$ and $b = 0$, $\Omega(E, 1, 0) = \frac{8\pi^2}{3} E^{3/2}$.

5. Mechanical cycle simulations and results

This section is divided into two subsections: subsection 5.1, where we present the energy variation in each step of the mechanical cycle, and subsection 5.2, where we present the energy variation in the entire mechanical cycle.

5.1. Energy variation in each step of the mechanical cycle

5.1.1. First step: During the first step of the mechanical cycle, the system goes from an ergodic state to an integrable one. Denote by E_1 the energy of a trajectory at the beginning of the first step and by E_2 the energy of this same trajectory at the end of

the first step. If adiabatic invariance holds true to the quasi-static evolution of this protocol, we know that

$$\Omega(E_1, 0.1, 0) = \Omega(E_2, 1, 0).$$

Using equation (4) and solving for E_2 ,

$$E_2 = \left(\frac{2f(0.1)}{\pi} \right)^{2/3} E_1, \quad (6)$$

where

$$f(a) = \sqrt{\frac{2}{1-a}} F \left(\sin^{-1} \sqrt{\frac{1-a}{1+a}} \middle| \frac{1+a}{1-a} \right).$$

It must be reiterated, however, that we can give no assurance to the validity of equation (6), as the Ergodic Adiabatic Theorem requires ergodicity to be on effect at all times of the evolution, and that is not the case here. We can, however, test this equation. Using a symplectic numerical integrator [38], we sampled 10^6 initial conditions with energy $E_1 = 0.5$ and evolved them in time with $b = 0$ and a increasing linearly from 0.1 to 1 in an elapsed time $\tau = 10^3 \tau_R$ (as we, of course, cannot achieve true quasi-staticity $\tau \rightarrow \infty$ in numerical simulations, we have to at least make sure that the switching time τ is much greater than a natural time scale of the system, and the relaxation time τ_R is a good contender for such a time scale). Figure 5 shows a histogram of energies of the aforementioned simulation. Even though the energies of the trajectories are not the same as the expected value, their average value (0.7896) agrees very well with the expected value (0.7870) from equation (6).

5.1.2. Second step: During the second step of the protocol, $a = 1$ at all times, while b increases (decreases) from 0 to b_M ($-b_M$). This means that the system is integrable at all times, and so we cannot use the Ergodic Adiabatic Theorem. However, there is a much simpler way to predict how the energy will change in this step.

Suppose a Hamiltonian can be written as

$$H(\mathbf{z}, \boldsymbol{\lambda}) = H_0(\mathbf{z}) + g(\alpha, \boldsymbol{\lambda}),$$

where g is a generic differentiable function, $\alpha = \alpha(\mathbf{z})$ is a constant of motion for the Hamiltonian H_0 (and, by extension, a constant of motion for H) and time dependence may be introduced through $\boldsymbol{\lambda} = \boldsymbol{\lambda}(t)$, the vector of external parameters. The energy difference of a trajectory, between times t_1 and t_2 , is

$$\Delta E = \int_{t_1}^{t_2} \frac{dH(\mathbf{z}, \boldsymbol{\lambda})}{dt} dt.$$

We know that $\frac{dH}{dt} = \frac{\partial H}{\partial t}$, so we can write

$$\Delta E = \int_{t_1}^{t_2} \frac{\partial H(\mathbf{z}, \boldsymbol{\lambda})}{\partial t} dt = \int_{t_1}^{t_2} \nabla_{\boldsymbol{\lambda}} g(\alpha, \boldsymbol{\lambda}) \cdot \frac{d\boldsymbol{\lambda}}{dt} dt,$$

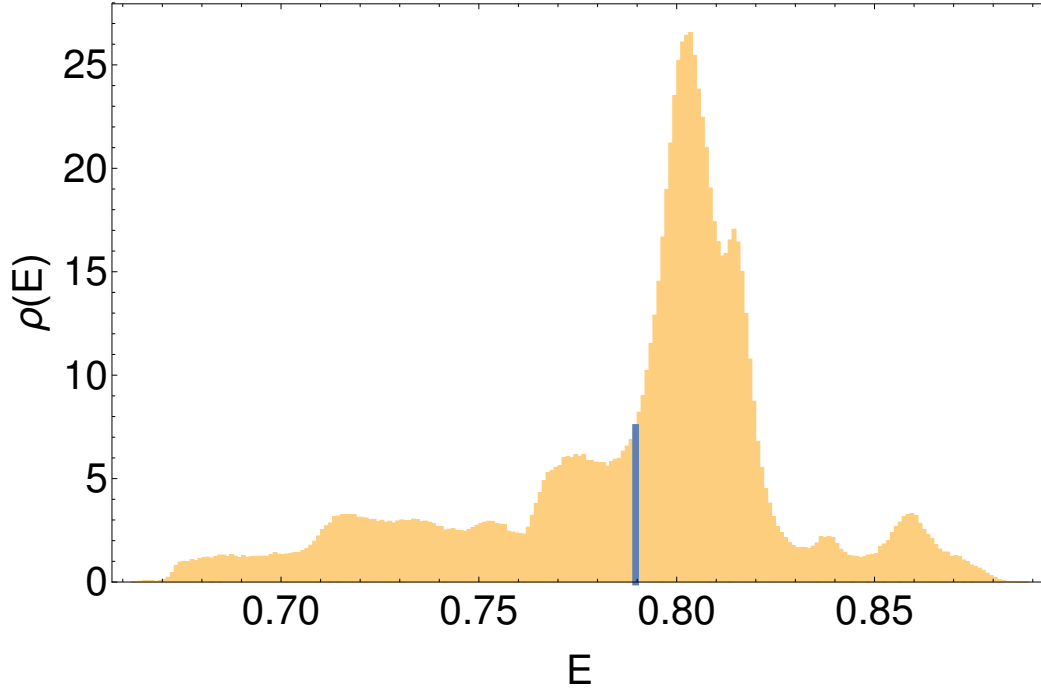


Figure 5. (Color online) Histogram of energies E after the first step of the mechanical cycle, where $\rho(E)$ is the energy distribution obtained from numerical simulations. We sampled 10^6 microcanonical initial conditions with energy $E = 0.5$ and evolved them by the first step of the protocol using the symplectic integrator of reference [38] in a simulation time of $\tau = 10^3 \tau_R$. Simulations with different switching times τ were conducted, but the general outline of the histograms are always the same. The blue line represents the expected energy value from the Ergodic Adiabatic Theorem. The average energy of the system after the evolution is 0.7896, in excellent agreement with the expected value 0.7870 from equation (6). Of course, the exact energy value of each trajectory after the evolution may not be close to the expected value, and that may be because this process is not perfectly adiabatic, as that would require $\tau \rightarrow \infty$.

where ∇_{λ} is the gradient operation with respect to λ and the last step was obtained using $\frac{d\alpha}{dt} = 0$, as we assumed from the beginning. Denoting $\lambda_i = \lambda(t_i)$, $i = 1$ or 2 , we get

$$\Delta E = \int_{\lambda_1}^{\lambda_2} \nabla_{\lambda} g(\alpha, \lambda) \cdot d\lambda = g(\alpha, \lambda_2) - g(\alpha, \lambda_1),$$

and the energy difference only depends on how g changes through the variation of $\lambda(t)$.

In our specific case, α is the angular momentum L , H_0 is the QS Hamiltonian with $a = 1$, $\lambda = b$ and $g(\alpha, \lambda) = bL$. If the energy of a trajectory at the beginning of step 2 is E_2 and at the end is E_3 , their difference is

$$E_3 = E_2 - |L|b_M, \quad (7)$$

and the energy of every trajectory always decreases after the second step, independent on the switching time τ . It should now be clear why we set up our mechanical cycle like we did: using the information acquired in the measurement of angular momentum, we

can make sure that all trajectories lose energy during the second step, and the bigger the angular momentum, the bigger the energy loss.

5.1.3. Third step: During the third step of the mechanical cycle, we again make use of the Ergodic Adiabatic Theorem. Denote by E_3 the energy of a trajectory at the beginning of the third step and by E_4 the energy of this same trajectory at the end of this same step. Then

$$\Omega(E_3, 1, \pm b_M) = \Omega(E_4, 0.1, 0).$$

Using equations (4) and (5) and solving for E_4 gives

$$E_4 = \left(\frac{\pi}{16f(0.1)} \left[(b_M^4 + 4E_3)^{3/2} + b_M^2 (b_M^4 + 6E_3) \right] \right)^{2/3}. \quad (8)$$

The mechanical cycle is finished.

5.2. Energy variation in the entire mechanical cycle

We can write the total energy variation $\Delta E = E_4 - E_1$ in the mechanical cycle as a function of the initial energy E_1 , the angular momentum L measured in the second step and b_M (from equations (6)-(8))

$$\begin{aligned} \Delta E(E_1, L, b_M) = & \left\{ \frac{\pi}{16f(0.1)} \left[\left(b_M^4 + 4 \left[\left(\frac{2f(0.1)}{\pi} \right)^{2/3} E_1 - |L|b_M \right] \right)^{3/2} \right. \right. \\ & \left. \left. + b_M^2 \left(b_M^4 + 6 \left[\left(\frac{2f(0.1)}{\pi} \right)^{2/3} E_1 - |L|b_M \right] \right) \right] \right\}^{2/3} - E_1. \end{aligned} \quad (9)$$

Even though this approach may be too simplistic, equation (9) can be compared to numerical simulations of the system. Using a symplectic integrator [38], we sampled 10^5 initial conditions for a few values of E_1 and evolved them through our mechanical cycle for a few values of b_M in $\tau = 10^3 \tau_R$ units of simulation time. Figure 6 shows, for each numerical simulation with E_1 and b_M given, the energy variation versus angular momentum measured of each initial condition, along with the theoretical prediction from equation (9). The sign of the theoretical average energy variations can be estimated from the area under the red curves in figure 6. This is so because the angular momentum distributions after the second step of the mechanical cycle do not show significant variation within the interval of allowed values of angular momentum and can be considered approximately uniform (see Appendix B). Hence, theoretical energy extraction can be easily visualized. We can see that, in figures 6a, 6d and 6e, the agreement between theory and data is far-fetched and the arrangement of points is too complicated to be well described by equation (9). However, in figure 6c and even more in figure 6b, although there is no complete agreement between the simulation data and the theoretical prediction, the majority of points lie around a curve that roughly follows the theoretical curve. These points present positive energy variation for low

values of angular momentum and negative energy variation for high values of angular momentum, conforming to what we predicted the second step of the mechanical cycle would do. There are also points that do not resemble the theoretical curve at all, forming a secondary curve that lies entirely below the horizontal axis $\Delta E = 0$, giving us initial conditions that lose energy during the mechanical cycle and that did not fit into our predictions. Figure 6b is also the one where the theoretical prediction of the average energy variation, $\langle \Delta E \rangle^{\text{the}}$ (see Appendix B to understand how $\langle \Delta E \rangle^{\text{the}}$ is calculated), shows the least amount of percentual error compared to the numerical average, $\langle \Delta E \rangle^{\text{num}}$ (obtained by simple arithmetic average of the 10^5 initial conditions), an error of approximately 9%. On the other hand, figure 6a shows the biggest error, approximately 375%.

Interestingly, data concurs with theory for all five numerical simulations in one aspect: the sign of the average energy variation. For two of the simulations, figures 6a and 6e, the average energy variation is positive, whereas, in the other three, it is negative. This shows that energy extraction is not possible for any value of E_1 and b_M . Nevertheless, for a certain value of E_1 , there always seems to exist more than one value of b_M that ensures negative energy variation. The disagreement between data and theory can be attributed to the non-ergodicity of our system during the majority of the mechanical cycle and to the possibility that our mechanical cycle might never be able to be implemented adiabatically due to the presence of phase-space separatrices. Not surprisingly, these two reasons are related to the two conditions necessary for the Ergodic Adiabatic Theory to hold true. It is indeed unexpected that there is any approximate agreement between our theoretical predictions and the numerical data.

From equation (9), we can determine the average energy variation in the mechanical cycle, given E_1 and b_M ,

$$\langle \Delta E \rangle^{\text{the}}(E_1, b_M) = \int \Delta E(E_1, L, b_M) \rho(L|E_2) dL, \quad (10)$$

where $\rho(L|E_2)$ is the angular momentum distribution for possible values of L of a trajectory after step 1 of the mechanical cycle, conditioned by that trajectory having energy E_2 , given by equation (B.1). Figure 7 shows a 3D plot of equation (10), together with a few contour lines. It shows that, no matter the value E_1 in the beginning of the mechanical cycle, there exists a value of b_M that ensures negative average energy variation.

The numerical simulations confirms that the microcanonical average of ΔE is smaller than zero for the specific values of initial energy E_1 and external parameter b_M we used. Even if that is not the case for all values of E_1 and b_M , the mere existence of a such an example defies the Kelvin-Planck statement of the Second Law of Thermodynamics, as argued in the Introduction.

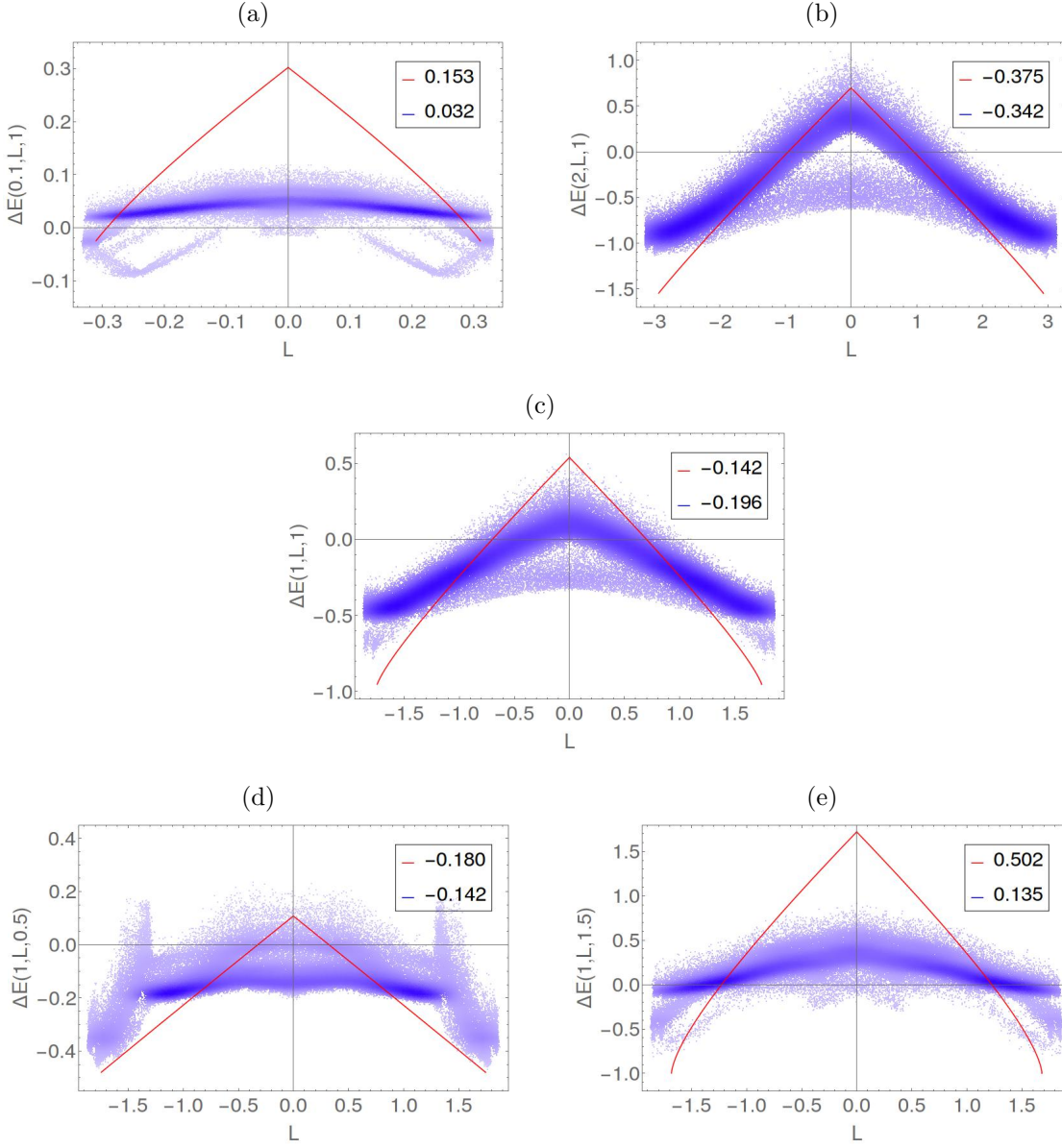


Figure 6. (Color online) Comparison of the theoretical prediction $\Delta E(E_1, L, b_M)$, given by equation (9), and the data obtained from numerical simulations for a few values of E_1 and b_M . In red, we have the energy variation versus angular momentum measured curve obtained by application the Ergodic Adiabatic Theorem and in blue we have the 10^5 initial conditions sampled, with higher density of points represented by darker shades of blue. The legends on each figure give the average energy variation, theoretical (red) and numerical (blue). The parameters used in each numerical simulation are: (a) $E_1 = 0.1$, $b_M = 1$; (b) $E_1 = 2$, $b_M = 1$; (c) $E_1 = 1$, $b_M = 1$; (d) $E_1 = 1$, $b_M = 0.5$; (e) $E_1 = 1$, $b_M = 1.5$.

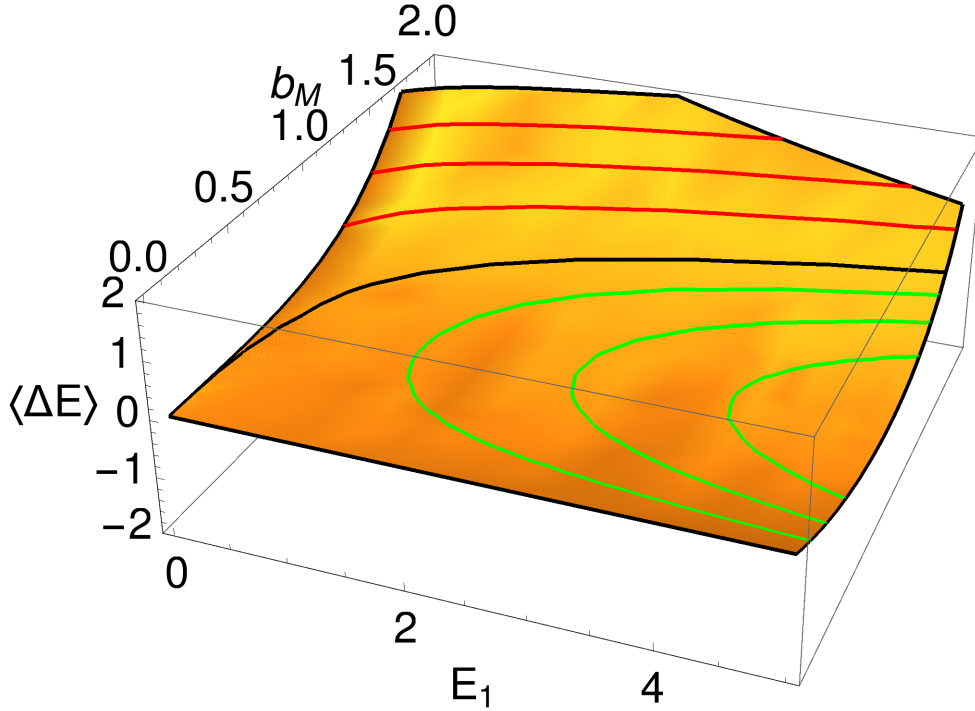


Figure 7. (Color online) 3D plot of the average expected energy variation from equation (10). The green lines are contour lines of negative energy variation, the red lines are contour lines of positive energy variation and the black line corresponds to no energy variation. The contour line of zero average energy variation is monotonic, which implies that, given E_1 , there is always a value of b_M that gives negative energy variation.

6. Discussion

Our model is very similar to the Microcanonical Szilárd Engines existent so far. With the same general setup as ours (starting with a system in contact with a heat reservoir, disconnecting them, acting on the system and finally reconnecting them), Vaikuntanathan and Jarzynski [31] devised a one-dimensional system in which they can consistently lower the system's energy in a feedback process with energy measurement, no matter the energy measured. The critical difference here is that our energy variation is only negative *on average*, while theirs is negative in every single realization of their process (at least in the quasi-static limit, some trajectories do gain energy for finite times). They too apply the Ergodic Adiabatic Theorem to show the extraction of energy and, in another instance [41], show that the presence of separatrices in phase-space during their process is crucial for their engine to work. Because of this, we believe that phase-space separatrices are relevant in our case too, but a more meticulous investigation would be required to understand the effects of separatrix crossings here, either in enabling negative average variation or in justifying the disagreement between data and theory in figure 6. One thing to note is that separatrices in our model ought to be much more complicated than those found in Vaikunthanathan and Jarzynski's model, where a closed form for

their equation can be found effortlessly. Studies of the effects of separatrix crossing in one-dimensional systems have been developed [42, 43], but not much has been done to multi-dimensional systems.

Our model has a lot in common with the original Szilárd Engine too. When the barrier is introduced in the Szilárd Engine, the particle “chooses” a side of the box and the phase space reflection symmetry with respect to the coordinate axis (a parity symmetry) is broken. Half of the phase space is essentially erased for that particular trajectory after the measurement. With the assistance of measurement, a protocol is carried out in order to abuse this lack of reflection symmetry and extract energy from the system. This may seem at odds with our model, because right before the measurement is made, when $a = 1$, a symmetry (angular momentum conservation) is established, not broken. Nonetheless, what matters here is the reflection symmetry that is broken when the particle “chooses” a certain value of angular momentum. After the measurement, step 2 of the mechanical cycle makes sure the energy of that specific trajectory decreases. In a way, we are using the two regions of positive and negative angular momentum of figure 2a as the two sides of the boxes of a Szilárd Engine, and it is precisely the conservation of angular momentum that allows us to brake the reflection symmetry. A key difference between our model and the original Szilárd Engine is that, in the original Szilárd Engine, the barrier insertion and removal have no energy costs, while the equivalent in our model (steps 1 and 3 of the evolution of external parameters, respectively) do come with energy variations.

It has been noted in reference [28] that examples of Szilárd engines, all of which include feedback processes, usually apply processes that violate either Liouville’s Theorem (like the original Szilárd Engine [2]) or the Ergodic Adiabatic Theorem (like the Microcanonical Szilárd Engine of reference [31]). Considering that these are the two theorems used to show the impossibility of energy extraction from a single heat reservoir in a cycle, it is no surprise that Szilárd engines violate the Kelvin-Planck statement of the second law. As mentioned in the Introduction, it has been shown, in a very general context, that the mistreatment of Liouville’s theorem in isothermal processes is linked to symmetry breaking [23, 27], in the sense that the phase-space loses a symmetry that the Hamiltonian has. Such an analysis has not yet been developed for thermally isolated processes, that happen without connection to a heat reservoir, like the processes carried out in Microcanonical Szilárd Engines.

However, there is a case to be made that separatrix crossing, present in Microcanonical Szilárd Engines, constitutes a kind of symmetry breaking. After all, separatrix crossing is a possible cause of sudden shrinkage of phase-space volume. Separatrix crossing symmetry breaking is not a symmetry breaking caused directly by an external agent like in the original Szilárd Engine, where the insertion of a barrier causes sudden shrinkage of phase space volume, but a symmetry breaking caused by the natural evolution of a time-dependent system. The external agent still acts indirectly, creating and destroying separatrices through the variation of external parameters and ultimately shrinking phase-space volume whenever a trajectory crosses a separatrix. In

the end, whenever an isolated system (and that may be system of interest plus heat reservoir) suddenly experiences a decrease in its phase-space volume Ω , as caused by any type of symmetry breaking, the system's entropy $S \propto \log \Omega$ will also decrease and it is easy to see how the Second Law of Thermodynamics fails, as per Planck's statement.

7. Conclusions

In this paper, we described how to build a system with two degrees of freedom that goes against the Kelvin-Planck statement of the Second Law of Thermodynamics. We used a theoretical tool, the Ergodic Adiabatic Theorem, and numerical simulations to motivate and show exactly how our model works. Our model is, by all means, a Maxwell Demon.

Reclaiming the Kelvin-Planck statement from the demon via Landauer's principle in our case is done in the same way Vaikuntanathan and Jarzyski [31] have done for their case. We can consider a finite precision energy measurement apparatus that saves the information acquired in each measurement in a certain number of bits. We then choose the value of our external parameter, b_M , based on this finite precision measurement, as with any feedback process. We can see, from figure 7, that it is always possible to choose a value of b_M that guarantees average energy extraction on average. Applying here the same reasoning given in section III of reference [31], which includes Landauer's principle, it follows that the maximum work extracted with finite precision measurements from the system only matches the minimum work required to erase the information contained in the bits. Even more energy would be necessary to erase the angular momentum information saved, as that would require one extra bit (the sign of the angular momentum can be positive or negative) per energy measurement.

Our results contrast with the results obtained by the authors of reference [37], regarding the *Fermi acceleration* phenomenon. They show that a particle in a two-dimensional time-dependent billiard, where the particle is constantly colliding with moving walls, has an exponential energy growth. The billiard oscillates cyclically and adiabatically, just as our system (and most Microcanonical Szilárd Engines) does. As we see it, there are two main differences: the absence of measurement in their system, and it is a well known fact that Szilárd Engines and Maxwell Demons all require information (i.e. feedback processes) to achieve their goal; and the absence of thermalization in their system, achieved in our system through the reconnection with the heat reservoir at the end of the thermodynamic cycle. It remains to be shown exactly how these differences bring forth such differing outcomes.

Whether or not the discussion of the previous section is enough to qualify our example (and Sato's example) as a Microcanonical Szilárd Engine is open to debate. Either way, in a sense, our example serves as a complement to the already established Microcanonical Szilárd Engines, showing that it is possible to conceive a system with more than one degree of freedom whose microcanonical average energy decreases after a cycle. The fact that such a system can exist even when non-integrability and chaos are present suggests that Microcanonical Szilárd Engines are not limited to microscopic

systems and that there should exist a way to explain Microcanonical Szilárd Engines through symmetry breaking.

Appendix A. Averages in the microcanonical ensemble

In this appendix, we show how to calculate microcanonical averages for the QS Hamiltonian given by equation (1)

$$H^{\text{QS}}(\mathbf{z}, a) = \frac{p_x^2}{2} + \frac{p_y^2}{2} + \frac{a}{4}(x^4 + y^4) + \frac{x^2 y^2}{2}. \quad (\text{A.1})$$

The microcanonical phase space distribution is

$$\rho(\mathbf{z}, E, a) = \frac{\delta(H^{\text{QS}}(\mathbf{z}, a) - E)}{\int \delta(H^{\text{QS}}(\mathbf{z}, a) - E) d\mathbf{z}}, \quad (\text{A.2})$$

where δ represents the Dirac delta function. For easier manipulation of this distribution, we define a non-canonical transformation from the canonical variables (x, p_x, y, p_y) to the non-canonical variables (H, ψ, θ, ϕ) :

$$\begin{aligned} x^2 &= \sqrt{\frac{2H}{\cos 2\theta}} \left(\frac{\cos \theta}{\sqrt{1+a}} + \frac{\sin \theta}{\sqrt{1-a}} \right) \sin \psi; \\ y^2 &= \sqrt{\frac{2H}{\cos 2\theta}} \left(\frac{\cos \theta}{\sqrt{1+a}} - \frac{\sin \theta}{\sqrt{1-a}} \right) \sin \psi; \\ p_x &= \sqrt{2H} \cos \phi \cos \psi; \\ p_y &= \sqrt{2H} \sin \phi \cos \psi, \end{aligned} \quad (\text{A.3})$$

with (H, ψ, θ, ϕ) well defined within $0 \leq H \leq \infty, 0 \leq \psi \leq \pi/2, 0 \leq \theta \leq \cos^{-1}(a)/2$ and $0 \leq \phi \leq 2\pi$. This way, the kinetic and potential parts of equation (A.1) can be written as

$$K = \frac{p_x^2}{2} + \frac{p_y^2}{2} = H \cos^2 \psi \quad (\text{A.4})$$

and

$$V = \frac{a}{4}(x^4 + y^4) + \frac{x^2 y^2}{2} = H \sin^2 \psi, \quad (\text{A.5})$$

while equation (A.2) simplifies to

$$\rho(H, E, a) = \frac{\delta(H - E)}{\int J(E, \psi, \theta, \psi) d\psi d\theta d\phi}, \quad (\text{A.6})$$

where

$$J(H, \psi, \theta, \phi) = \sqrt{\frac{H}{2(\cos 2\theta - a) \cos 2\theta}} \cos \psi$$

is the Jacobian of the non-canonical transformation defined by equation (A.3). The average kinetic energy is then, with help from equations (A.4) and (A.6),

$$\begin{aligned} \langle K \rangle(E, a) &= \int K \rho(\mathbf{z}, E, a) d\mathbf{z} \\ \langle K \rangle(E, a) &= \frac{1}{\int J(E, \psi, \theta, \psi) d\psi d\theta d\phi} \int H \cos^2 \psi \delta(H - E) J(H, \psi, \theta, \phi) dH d\psi d\theta d\phi \\ \langle K \rangle(E, a) &= E \int_0^{\pi/2} \cos^3 \psi d\psi = \frac{2E}{3}. \end{aligned}$$

Likewise, from equations (A.5) and (A.6), the average potential energy is

$$\langle V \rangle(E, a) = E \int_0^{\pi/2} \sin^2 \psi \cos \psi d\psi = \frac{E}{3}.$$

Non surprisingly, we have $\langle K \rangle + \langle V \rangle = E$.

Appendix B. Angular momentum distribution

In this appendix, we will show the angular momentum distribution for the Hamiltonian of equation (1) and how it is used to calculate theoretical average energy variations in our mechanical cycle.

Assuming the Ergodic Adiabatic Theorem holds true, every trajectory that starts the mechanical cycle with energy E_1 will reach the end of the first step of the mechanical cycle with energy E_2 , given by equation (6). The angular momentum distribution $\rho(L|E_2)$ for possible values of angular momentum L of the trajectories, conditioned by having energy E_2 at the end of the first step, is

$$\rho(L|E_2) = \frac{1}{\omega(E_2, 1)} \int \delta(E_2 - H^{\text{QS}}(\mathbf{z}, 1)) \delta(L - (xp_y - yp_x)) dz, \quad (\text{B.1})$$

where $\omega(E, a) = \int \delta(E - H^{\text{QS}}(\mathbf{z}, a)) dz$ is the density of states of energy E and δ is the Dirac Delta function. This distribution is nothing more than the summation of contributions of all trajectories with angular momentum L weighted by the microcanonical distribution $\frac{1}{\omega(E, a)} \delta(E - H^{\text{QS}}(\mathbf{z}, a))$. The average energy variation of the mechanical cycle is then given by equation (10).

Figure B1 shows the distribution of equation (B.1) for $E_1 = 0.5$ (figure B1a) and $E_1 = 2$ (figure B1b), together with histograms of angular momenta after the first step of the mechanical cycle described in section 4, obtained through numerical simulations. We can also see that the theoretical curves deviate a lot from the numerical simulations, which might be a sign of separatrix crossing invalidating the Ergodic Adiabatic Theorem.

Acknowledgments

The authors acknowledge support from FAPESP/CAPES, grant #2016/19631-9, São Paulo Research Foundation (FAPESP).

References

- [1] Maxwell J C, *Theory of Heat*, 1871 Longmans
- [2] Szilárd L, *Über die Entropieverminderung in einem thermodynamischen System bei Eingriffen intelligenter Wesen*, 1929 *Zeitschrift für Physik* **53** 840
- [3] Landauer R, *Irreversibility and Heat Generation in the Computing Process*, 1961 *IBM Journal of Research and Development* **5** 183
- [4] Bennett C H, *The thermodynamics of computation—a review*, 1982 *International Journal of Theoretical Physics* **21** 905

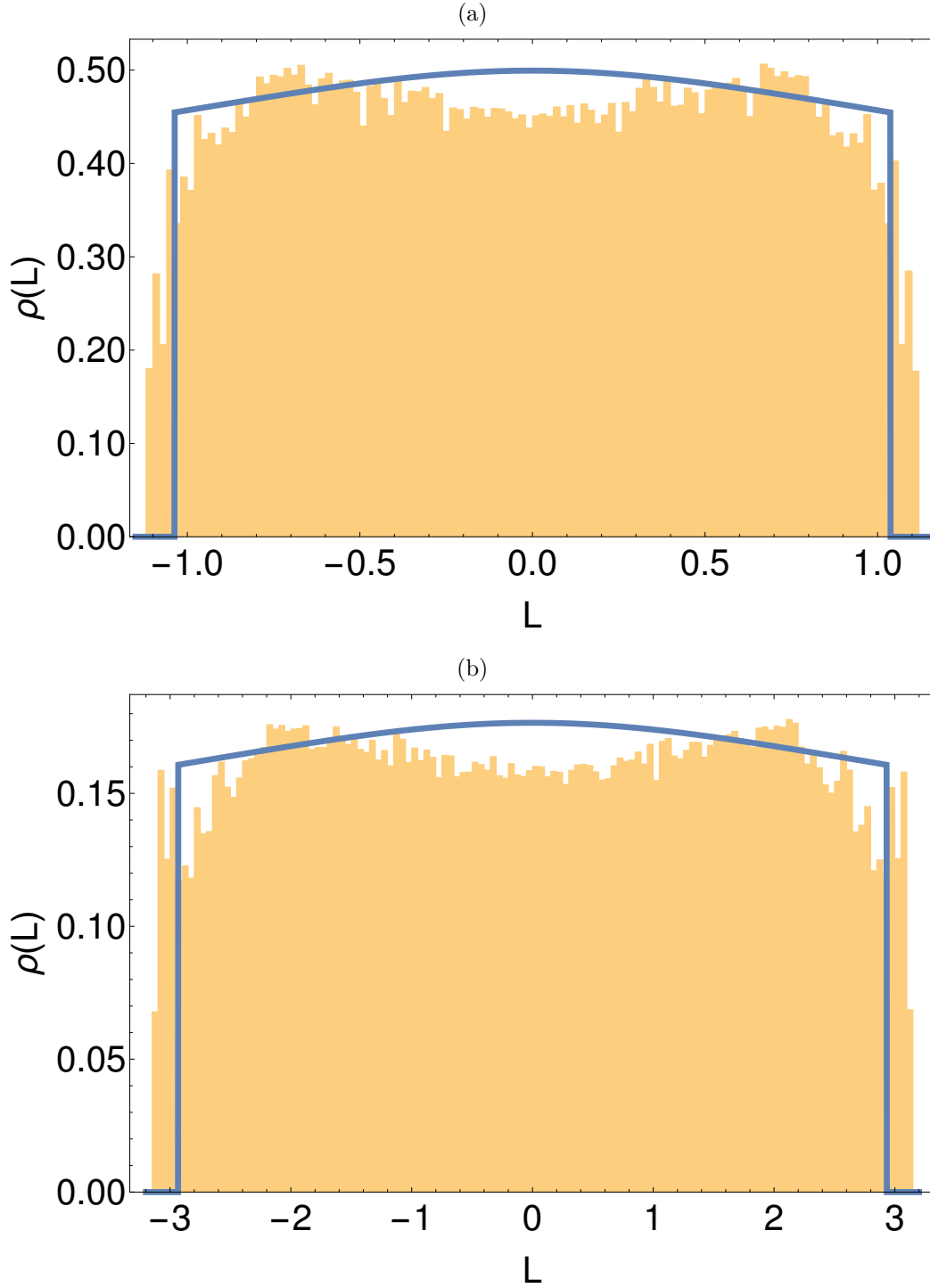


Figure B1. (Color online) Histograms of angular momentum L after the first step of the mechanical cycle for (a) $E_1 = 0.5$ and (b) $E_1 = 2$, where $\rho(L)$ is the angular momentum distribution. The blue curves represent the expected angular momentum distribution from the Ergodic Adiabatic Theorem, equation (B.1). The sudden drop to zero is expected: L has a maximum and a minimum possible value as functions of the system's energy E_2 , given by $L^{\max} = \left(\frac{4E_2}{3}\right)^{3/4}$, and so this distribution should be zero for values outside the range $-L^{\max} < L < L^{\max}$.

- [5] Sagawa T and Ueda M, *Second Law of Thermodynamics with Discrete Quantum Feedback Control*, 2008 *Phys. Rev. Lett.* **100** 080403
- [6] Sagawa T and Ueda M, *Minimal Energy Cost for Thermodynamic Information Processing: Measurement and Information Erasure*, 2009 *Phys. Rev. Lett.* **102** 250602
- [7] Sagawa T and Ueda M, *Generalized Jarzynski Equality under Nonequilibrium Feedback Control*, 2010 *Phys. Rev. Lett.* **104** 090602
- [8] Sagawa T and Ueda M, *Nonequilibrium thermodynamics of feedback control*, 2012 *Phys. Rev. E* **85** 021104
- [9] Sagawa T, *Thermodynamics of Information Processing in Small Systems*, 2012 Springer Japan
- [10] Price G N, Bannerman S T, Viering K, Narevicius E and Raizen M G, *Single-Photon Atomic Cooling*, 2008 *Phys. Rev. Lett.* **100** 093004
- [11] Cao F J and Feito M, *Thermodynamics of feedback controlled systems*, 2009 *Phys. Rev. E* **79** 041118
- [12] Bannerman S T, Price G N, Viering K and Raizen M G, *Single-photon cooling at the limit of trap dynamics: Maxwell's demon near maximum efficiency*, 2009 *New Journal of Physics* **11** 063044
- [13] Jacobs K, *Second law of thermodynamics and quantum feedback control: Maxwell's demon with weak measurements*, 2009 *Phys. Rev. A* **80** 012322
- [14] Ponmurugan M, *Generalized detailed fluctuation theorem under nonequilibrium feedback control*, 2010 *Phys. Rev. E* **82** 031129
- [15] Horowitz J M and Vaikuntanathan S, *Nonequilibrium detailed fluctuation theorem for repeated discrete feedback*, 2010 *Phys. Rev. E* **82** 061120
- [16] Abreu D and Seifert U, *Extracting work from a single heat bath through feedback*, 2011 *EPL (Europhysics Letters)* **94** 10001
- [17] Mandal D and Jarzynski C, *Work and information processing in a solvable model of Maxwell's demon*, 2012 *Proceedings of the National Academy of Sciences* **109** 11641
- [18] Barato A C and Seifert U, *An autonomous and reversible Maxwell's demon*, 2013 *EPL (Europhysics Letters)* **101** 60001
- [19] Deffner S and Jarzynski C, *Information Processing and the Second Law of Thermodynamics: An Inclusive, Hamiltonian Approach*, 2013 *Phys. Rev. X* **3** 041003
- [20] Barato A C and Seifert U, *Unifying Three Perspectives on Information Processing in Stochastic Thermodynamics*, 2014 *Phys. Rev. Lett.* **112** 090601
- [21] Lu Z, Mandal D and Jarzynski C, *Engineering Maxwell's demon*, 2014 *Phys. Today* **67(8)** 60
- [22] Kim S W, Sagawa T, De Liberato S and Ueda M, *Quantum Szilard Engine*, 2011 *Phys. Rev. Lett.* **106** 070401
- [23] Roldán É, Martínez I A, Parrondo J M R and Petrov D, *Universal features in the energetics of symmetry breaking*, 2014 *Nature Physics* **10** 457
- [24] Toyabe S, Sagawa T, Ueda M, Muneyuki E and Sano M, *Experimental demonstration of information-to-energy conversion and validation of the generalized Jarzynski equality*, 2010 *Nature Physics* **6** 988
- [25] Koski J V, Maisi V F, Sagawa T and Pekola J P, *Experimental Observation of the Role of Mutual Information in the Nonequilibrium Dynamics of a Maxwell Demon*, 2014 *Phys. Rev. Lett.* **113** 030601
- [26] Koski J V, Maisi V F, Pekola J P and Averin D V, *Experimental realization of a Szilard engine with a single electron*, 2014 *Phys. Rev. Lett.* **111** 13786
- [27] Parrondo J M R, *The Szilard engine revisited: Entropy, macroscopic randomness, and symmetry breaking phase transitions*, 2001 *Chaos* **11** 725
- [28] Parrondo J M R and Granger L, *Maxwell demons in phase space*, 2015 *Eur. Phys. J. Spec. Top.* **224** 865
- [29] Sato K, *An Example of a Mechanical System whose Ensemble Average Energy, Starting with a Microcanonical Ensemble, Decreases after an Operation*, 2002 *Journal of the Physical Society of Japan* **71** 1065

- [30] Marathe R and Parrondo J M R, *Cooling Classical Particles with a Microcanonical Szilard Engine*, 2010 *Phys. Rev. Lett.* **104** 245704
- [31] Vaikuntanathan S and Jarzynski C, *Modeling Maxwell's demon with a microcanonical Szilard engine*, 2011 *Phys. Rev. E* **83** 061120
- [32] Acconcia T V and Bonança M V S, *Microcanonical Szilárd engines beyond the quasistatic regime*, 2017 *Phys. Rev. E* **96** 062117
- [33] Allahverdyan A E and Hovhannisyan K V, *Work extraction from microcanonical bath*, 2011 *EPL (Europhysics Letters)* **95** 60004
- [34] Carnegie A and Percival I C, *Regular and chaotic motion in some quartic potentials*, 1984 *Journal of Physics A: Mathematical and General* **17** 801
- [35] Lichtenberg A J and Lieberman M A, *Regular and chaotic dynamics*, 1992 Springer-Verlag
- [36] Bonança M V S, *Relaxation in finite and isolated classical systems: An extension of Onsager's regression hypothesis*, 2012 *Phys. Rev. E* **85** 031122
- [37] Gelfreich V, Rom-Kedar V, Shah K Turaev D, *Robust Exponential Acceleration in Time-Dependent Billiards*, 2011 *Phys. Rev. Lett.* **106** 801
- [38] Forest E and Ruth R D, *Fourth-order symplectic integration*, 1990 *Physica D: Nonlinear Phenomena* **1** 105
- [39] Reggie B, Ott E and Grebogi C, *Ergodic adiabatic invariants of chaotic systems*, 1987 *Phys. Rev. Lett.* **59** 1173
- [40] Ott E, *Goodness of Ergodic Adiabatic Invariants*, 1979 *Phys. Rev. Lett.* **42** 1628
- [41] Lu Z, Jarzynski C and Ott E, *Apparent topologically forbidden interchange of energy surfaces under slow variation of a Hamiltonian*, 2015 *Phys. Rev. E* **91** 052913
- [42] Tennyson J L, Cary J R and Escande D F, *Change of the Adiabatic Invariant due to Separatrix Crossing*, 1986 *Phys. Rev. Lett.* **56** 2117
- [43] Cary J R, Escande D F and Tennyson J L, *Adiabatic-invariant change due to separatrix crossing*, 1986 *Phys. Rev. A* **34** 4256